

## Noise suppression in a temporal-multimode quantum memory entangled with a photon via an asymmetrical photon-collection channel

Ya Li , Ya-fei Wen, Min-jie Wang, Chao Liu, Hai-long Liu, Shu-jing Li, Zhong-xiao Xu, and Hai Wang\*

*The State Key Laboratory of Quantum Optics and Quantum Optics Devices, Institute of Opto-Electronics, Collaborative Innovation Center of Extreme Optics, Shanxi University, Taiyuan 030006, People's Republic of China*



(Received 26 January 2022; revised 5 June 2022; accepted 20 July 2022; published 15 August 2022)

Quantum interfaces (QIs) that generate entanglement between a multimode atomic memory and a photon form a multiplexed repeater node and could greatly improve quantum repeater rates. Recently, a temporal multimode spin-wave memory entangled with a photon was demonstrated with cold atoms [Wen *et al.*, *Phys. Rev. A* **100**, 012342 (2019)]. However, due to the additional noise generated in a multimode operation, the fidelity of the spin-wave–photon entanglement significantly decreases with the mode number. So far, improvements in the temporal-multimode entanglement fidelity associated with suppressing the additional noise have not been explored. In this work, we propose and experimentally demonstrate a scheme that can suppress the additional noise of a temporally multiplexed QI. The scheme uses an asymmetric channel to retrieve the photons coming from the temporally multiplexed QI. For comparison purposes, we also set up a QI that uses a symmetric channel for photon collection. When the QIs store 14 modes, the measured Bell parameters  $S$  for the QIs using the asymmetric and the symmetric photon-collection channels are  $2.36 \pm 0.03$  and  $2.24 \pm 0.04$ , respectively, which means that a QI using an asymmetric channel provides a 3% increase in the entanglement fidelity, i.e., a 1.7-fold decrease in the additional noise, compared with a QI using a symmetric channel. In addition, the 14-mode entanglement QIs that use the asymmetric and symmetric collections preserve the violation of a Bell inequality for storage times of up to  $\sim 25$  and  $\sim 20$   $\mu\text{s}$ , respectively, showing that the asymmetric QI has better entanglement storage performance.

DOI: [10.1103/PhysRevA.106.022610](https://doi.org/10.1103/PhysRevA.106.022610)

### I. INTRODUCTION

Large-scale quantum networks [1–3] and long-distance quantum communication [3–5] rely on long-distance entanglement distribution through quantum repeaters (QRs) [6]. In QRs [4–6], the long-distance  $L$  over which one wants to distribute entanglement is divided into short elementary links. Each link contains two nodes with a separation distance  $L$ . Entanglement is generated in each short interval and then extended to the whole distance  $L$  through entanglement swapping [6]. The key element of each node is a light-matter quantum interface (QI) that generates quantum correlations or entanglement between an atomic memory and a photon [4,5]. To practically realize QRs, Duan, Lukin, Cirac, and Zoller (DLCZ) proposed a protocol [5] in which atom-photon quantum correlations can be created via spontaneous Raman scattering (SRS) induced by a write laser pulse in atomic ensembles, and such atom-photon quantum correlations have indeed been demonstrated [7–20]. Building on these atom-photon quantum correlations, many experiments have demonstrated the generation of atom-photon entanglement [21–31]. When using atom-photon entanglement instead of atom-photon quantum correlation for the repeater nodes, the long-distance phase stability required in the DLCZ protocol [5] is no longer necessary [32,33]. Alternatively, the

atom-photon entanglement QI may be generated through the storage of photonic entanglement [34–36] in atomic ensembles. With an atom-photon entanglement QI, quantum teleportation from photons [37,38] to matter [39] and entanglement generation for individual elementary links [40,41] have been demonstrated. However, it has been noted that DLCZ-type QRs based on single-mode storage have very slow rates for practical use [4,42–46]. One promising method for overcoming this problem is to use multimode QRs (nodes) instead of single-mode QRs to increase the elementary entanglement generation rate [44–48]. If the QRs use QIs capable of storing  $N$  modes as nodes, the repeater rate will be increased by a factor of  $N$  compared with that of those using single-mode QIs as nodes. In recent years, the temporally [49–57], spatially [48,58–61], and spectrally [47,62,63] multiplexed storage of weak coherent light or optical quantum states has been successfully demonstrated with solid-state and gas-state ensembles of atoms. With rare-earth ion-doped crystals [56,64] (solid-state atomic ensembles), spin-wave–photon quantum correlations in more than ten temporal modes have been demonstrated [56,57,65] via the DLCZ approach. Using multiple spatial-channel collections at the same time, multiplexed QIs that generate entanglement between a spin-wave qubit and a photonic qubit in six modes have been demonstrated with a cold atomic ensemble [48]. By using a two-dimensional acoustic-optic deflector to vary the spatial direction of a write laser beam, Duan’s group demonstrated a multiplexed DLCZ memory with 225 individual memory

\*wanghai@sxu.edu.cn

cells (modes) in a cold atomic ensemble [61]. By applying a train of write pulses with each pulse coming from a different direction to induce DLCZ Raman processes, multiplexed spin-wave–photon entanglement with 19 temporal storage modes has been achieved [55]. In addition, by applying a reversible external magnetic field with a gradient to control the rephasing of spin waves, the group of de Riedmatten demonstrated the generation of two time-separated spin waves in a cold atomic ensemble [66]. When comparing temporal and spatial multimode QIs, one can see that the photons from temporal-multimode QIs are collected and detected in a single optical channel (mode), while the photons from spatial-multimode QIs are collected and detected in multiple individual channels. Thus, temporal-multimode QIs reduce physical resources compared to spatial-multimode QIs. However, temporal-multimode QIs have the additional weakness [67,68] of additional noise induced by temporal-multimode spin waves [55]. This additional noise linearly increases with the storage mode number  $m$  and significantly decreases atom-photon quantum correlations and entanglement fidelity when the multiplexed memories have large-scale mode numbers. For example, in a temporal-multimode spin-wave–photon entanglement experiment [55], the dependence of the Bell parameter  $S$  on the mode number  $m$  shows that  $S$  decreases linearly with  $m$ . More precisely, when  $m = 1$ , the measured  $S = 2.65 \pm 0.03$ , and when  $m = 14$ , the measured  $S = 2.35 \pm 0.05$ . In the construction of QRs, improvements in the entanglement fidelity are crucially needed. Many experiments [69–72] have demonstrated entanglement purity from two initial entanglement sources. In several representative experiments, the improvements in the entanglement fidelity ( $F$ ) in the purified state were in the range of 5–10% better than the original entanglement states [69–71]. For temporally multiplexed DLCZ-type quantum memories, the mechanism behind the additional noise generated in the multimode operations was initially described by Simon *et al.* [46]. They also pointed out that the additional noise may be suppressed by using an optical cavity resonating with “write-out” photons but not resonating with “read-out” photons. Although the proposed scheme [46] can effectively reduce the additional noise, it excludes cavity-enhanced readout [27]. Following the above cavity scheme, de Riedmatten’s group experimentally demonstrated the improvement in nonclassical atom-photon correlations in temporally multiplexed DLCZ quantum memories (QMs) [73]. So far, improvements in the entanglement fidelity of temporally multiplexed atom-photon QIs have not been reported.

In the present work, we propose and experimentally demonstrate an approach to suppress the additional noise in a temporally multiplexed temporally multiplexed atom-photon entanglement QI. We generate entanglement between a temporal-multimode spin-wave QM and a Stokes photon following our previous experimental scheme [55]. In contrast to our previous work, in which only the symmetric channel was set up to collect the Stokes (write-out) and anti-Stokes (read-out) photons, the present approach involves setting up an asymmetric channel and a symmetric channel to collect the Stokes and anti-Stokes photons, respectively. The symmetric channel means that the Stokes and anti-Stokes modes have the same transverse spatial extent, and the asymmetric

channel means that the Stokes and anti-Stokes collection mode sizes differ [see Fig. 1(b) for details]. When the QIs store 14 modes, the measured Bell parameters  $S$  for the QIs using the asymmetric and the symmetric photon-collection channels are  $2.36 \pm 0.03$  and  $2.24 \pm 0.04$ , respectively, showing that the QI using the asymmetric channel gives rise to an increase of 0.12 in the Bell parameter. In contrast to the scheme proposed in Ref. [46], the present temporally multiplexed scheme does not exclude the improvement of the retrieval efficiency via a cavity-enhanced atom-photon coupling [27].

## II. EXPERIMENTAL SCHEME AND SETUP

We now describe a scheme to suppress the additional noise in a DLCZ-like temporally multiplexed quantum memory and improve the fidelity of the temporal-multimode atom-photon entanglement. The schematic experimental setup is shown in Fig. 1(a). The relevant levels of the  $^{87}\text{Rb}$  atoms are shown in Fig. 1(d), where  $|g\rangle = |5S_{1/2}, F_g = 1\rangle$ ,  $|s\rangle = |5S_{1/2}, F_s = 2\rangle$ ,  $|e_1\rangle = |5P_{1/2}, F_{e_1} = 1\rangle$ , and  $|e_2\rangle = |5P_{1/2}, F_{e_2} = 2\rangle$ . The time sequence of the experimental cycle is shown in Fig. 1(e). The repetition rate of the experimental cycle is  $\sim 30$  Hz (33 ms per cycle). In each cycle, the magneto-optical trap (MOT) is switched on for 23 ms for the preparation of the cold atoms and switched off for 10 ms for the generation of spin-wave–photon entanglement. After the cloud of cold atoms is released from the MOT, we prepare the atoms in the ground state  $|g\rangle$  via optical pumping with a clean laser pulse and then start the generation of temporal-multimode spin-wave–photon entanglement (SWPE). In each generation trial, we apply a train of write pulses labeled as  $W(t_i)$  ( $i = 1$  to  $m$ ), with each pulse coming from a different direction around the  $x$  axis onto the atoms [see Fig. 1(a)]. The write laser is  $\sigma^+$  polarized and blue detuned from the  $|g\rangle \rightarrow |e_2\rangle$  transition by 20 MHz. The duration of each write pulse is 70 ns. The time interval between two adjacent write pulses is 360 ns. The angular separation between the  $x$  axis and  $\text{CH}_{\alpha=1}$  ( $\text{CH}_{\alpha=2}$ ) is about  $2^\circ$  ( $-2^\circ$ ). Each write pulse induces spontaneous emission of Raman photons and simultaneously creates a DLCZ memory (spin wave). Such Raman photons are called Stokes photons or write-out photons. As shown in Fig. 1(a), we collected Stokes photons in two channels—the asymmetric collection channel [see Fig. 1(b)] and the symmetric collection channel [see Fig. 1(c)], labeled as  $\text{CH}_{\alpha=1}$  and  $\text{CH}_{\alpha=2}$ , respectively. The asymmetric and symmetric channels are both prealigned with light beams. For the asymmetric channel, a light beam emitted from the fiber collimator  $\text{FC}_{S1}$  passes through a lens and then goes through the atoms. The spot size of the light beam at the location of  $\text{FC}_{S1}$ , called the optical collection diameter  $d_{w,1}$  of  $\text{FC}_{S1}$ , is  $\sim 2.6$  mm. The focus length of the lens is  $f = 2.4$  m. At the atomic center, the light beam has a spot size of  $\sim 1.37$  mm. It is focused down to a spot of waist diameter 0.92 mm at a location 2.3 m away from  $\text{FC}_{S1}$  [see Fig. 1(b) for details]. Finally, the light beam is coupled to the fiber collimator  $\text{FC}_{AS1}$  (PAF-X-7-B, Thorlabs). At the position of  $\text{FC}_{AS1}$ , the light beam has a spot size of  $\sim 1.3$  mm, which is called the optical collection diameter  $d_{r,1}$  of  $\text{FC}_{AS1}$ . The coupling efficiency is up to 80%. For the symmetric channel [see Fig. 1(c)], a light beam emitted from the fiber collimator  $\text{FC}_{S2}$  directly passes



We use a single-photon detector  $D_w^\alpha$  ( $D_{w_1}^\alpha$  or  $D_{w_2}^\alpha$ ), which is shown in Fig. 1(a) (see below for details) to detect the Stokes photons. As shown in the time sequence of Fig. 1(e), the counts of the detectors  $D_{w_1}^\alpha$  and  $D_{w_2}^\alpha$  are registered only during the time bins  $S_\alpha(t_1) \cdots S_\alpha(t_i) \cdots S_\alpha(t_m)$ . When a Stokes photon is detected in the mode  $S_\alpha(t_i)$ , the storage of the spin wave in the mode  $k_{M_\alpha}(t_i) = k_w(t_i) - k_{S_\alpha}(t_i)$  is heralded. After a storage time  $t$ , the read laser pulse  $R_i$ , with its frequency that of the  $|s\rangle \rightarrow |e_1\rangle$  transition and its direction along  $-k_w(t_i)$ , is switched on by a feed-forward signal produced by a field-programmable gate array (FPGA), which converts the spin wave  $k_{M_\alpha}(t_i)$  into an anti-Stokes photon with its wave vector determined by the phase-matched condition  $k_{AS_\alpha} = k_w(t_i) - k_{S_\alpha} + k_{R_i} \approx -k_{S_\alpha}$ , where  $k_{R_i}$  denotes the wave vector of the read laser pulse  $R_i$  and satisfies  $k_{R_i} = -k_w(t_i)$ ,  $k_{S_\alpha}(t_1) = k_{S_\alpha}(t_2) = \dots = k_{S_\alpha}(t_m) = k_{S_\alpha}$ , meaning that the retrieved anti-Stokes photon propagates along the opposite direction to the Stokes photons. The duration of the read laser pulse is 70 ns. If two Stokes photons are detected in the modes  $S_\alpha(t_l)$  and  $S_\alpha(t_k)$  during the application of one write-pulse train ( $l, k \in m$  and  $l < k$ ), only the detection event in  $S_\alpha(t_l)$  is registered by the FPGA. The read laser pulse  $R_l$  with direction  $k_{R_l} = -k_{w_l}$  is controlled by the signal from the FPGA, and is switched on. The excitation in the  $M_\alpha(t_l)$  mode is converted into an anti-Stokes photon. After the retrieval, a clean pulse with a duration of 200 ns is applied to pump the atoms into the initial level  $|g\rangle$  and then the next trial of spin-wave-photon entanglement generation begins. If no Stokes photon is detected during the  $m$  write pulses, the atoms are pumped directly back into the initial level by the read and clean pulses. The subsequent trial then starts.

In the  $\text{CH}_\alpha$  channel, the Stokes (anti-Stokes) photons emitted (retrieved) by the atoms are initially collected by the fiber collimator  $\text{FC}_{S_\alpha}$  ( $\text{FC}_{AS_\alpha}$ ), as shown in Figs. 1(b) and 1(c).

They are then directed into an optical filter composed of several Fabry-Perot etalons. After the etalons, the  $\sigma^+$  ( $\sigma^-$ )-polarized Stokes (anti-Stokes) photons in the  $\text{CH}_1$  or  $\text{CH}_2$  channel are transformed into  $H(V)$ -polarized photons after passing a  $\lambda/4$  plate. The Stokes (anti-Stokes) photons then pass through a phase compensator [labeled PC in Fig. 1(a)], which can eliminate the phase shifts between the  $H$ - and  $V$ -polarized light fields resulting from optical elements such as optical fibers and filters. Subsequently, the Stokes (write-out) photons or anti-Stokes (read-out) photons go through a half-wave plate labeled as HWP in Fig. 1(a) and are guided into a polarization-beam splitter that transmits horizontal polarization and reflects vertical polarization into the single-photon detectors  $D_{w_1}^\alpha$  and  $D_{w_2}^\alpha$  or  $D_{r_1}^\alpha$  and  $D_{r_2}^\alpha$ , respectively.

Before detection, the write-out and read-out photons are in an entanglement state  $|\Phi_{pp}\rangle_\alpha^i = \cos \vartheta |H\rangle_{S_\alpha}^i |H\rangle_{AS_\alpha}^i + \sin \vartheta |V\rangle_{S_\alpha}^i |V\rangle_{AS_\alpha}^i$ , where  $|H\rangle_{S_\alpha}^i$  ( $|V\rangle_{S_\alpha}^i$ ) denotes an  $H$  ( $V$ )-polarized Stokes photon in the  $S_\alpha(t_i)$  mode and  $|H\rangle_{AS_\alpha}^i$  ( $|V\rangle_{AS_\alpha}^i$ ) denotes an  $H$  ( $V$ )-polarized anti-Stokes photon retrieved from the spin wave  $M_\alpha(t_i)$ . Note that the  $\sigma^+$  ( $\sigma^-$ ) polarization of the Stokes (anti-Stokes) photons in the  $\text{CH}_\alpha$  channel is transformed into  $H$  ( $V$ ) polarization by the  $\lambda/4$  plate mentioned above.

The quality of the atom-photon (photon-photon) entanglement created from the temporally multiplexed QI storing  $m$  spin-wave modes in  $\text{CH}_\alpha$  can be characterized by the Bell parameter:

$$S_\alpha^{(m)} = |E_\alpha^{(m)}(\theta_S, \theta_{AS}) - E_\alpha^{(m)}(\theta_S, \theta'_{AS}) + E_\alpha^{(m)}(\theta'_S, \theta_{AS}) + E_\alpha^{(m)}(\theta'_S, \theta'_{AS})| < 2, \quad (4)$$

with the correlation function  $E_\alpha^{(m)}(\theta_S, \theta_{AS})$  given by

$$\frac{C_{D_{w_1}^\alpha, D_{r_1}^\alpha}^{(m)}(\theta_S, \theta_{AS}) + C_{D_{w_2}^\alpha, D_{r_2}^\alpha}^{(m)}(\theta_S^\perp, \theta_{AS}^\perp) - C_{D_{w_2}^\alpha, D_{r_1}^\alpha}^{(m)}(\theta_S^\perp, \theta_{AS}) - C_{D_{w_1}^\alpha, D_{r_2}^\alpha}^{(m)}(\theta_S, \theta_{AS}^\perp)}{C_{D_{w_1}^\alpha, D_{r_1}^\alpha}^{(m)}(\theta_S, \theta_{AS}) + C_{D_{w_2}^\alpha, D_{r_2}^\alpha}^{(m)}(\theta_S^\perp, \theta_{AS}^\perp) + C_{D_{w_2}^\alpha, D_{r_1}^\alpha}^{(m)}(\theta_S^\perp, \theta_{AS}) + C_{D_{w_1}^\alpha, D_{r_2}^\alpha}^{(m)}(\theta_S, \theta_{AS}^\perp)}, \quad (5)$$

where, for example,  $C_{D_{w_1}^\alpha, D_{r_1}^\alpha}^{(m)}(\theta_S, \theta_{AS}) = \sum_{i=1}^m C_{D_{w_1}^\alpha, D_{r_1}^\alpha}^{(i-h)}(\theta_S, \theta_{AS})$ ,  $C_{D_{w_1}^\alpha, D_{r_1}^\alpha}^{(i-h)}(\theta_S, \theta_{AS})$  denotes the coincidence counts between the detection of a Stokes photon in the time bin  $S_\alpha(t_i)$  by  $D_{w_1}^\alpha$  and the detection of a retrieved anti-Stokes photon from  $M_\alpha(t_i)$  by  $D_{r_1}^\alpha$  for polarization angles  $\theta_S$  and  $\theta_{AS}$ . The polarization angles  $\theta_S$  ( $\theta_{AS}$ ) of the Stokes (anti-Stokes) photons can be set by the  $\lambda/2$  HWP mentioned above. In the measurement, the canonical settings are chosen to be  $\theta_S = 0^\circ$ ,  $\theta'_S = 45^\circ$ ,  $\theta_{AS} = 22.5^\circ$ , and  $\theta'_{AS} = 67.5^\circ$ , with  $\theta_S^\perp = \theta_S + \pi/2$  ( $\theta_{AS}^\perp = \theta_{AS} + \pi/2$ ). The coincidence  $C(\theta_S, \theta_{AS})$  of single-mode entanglement for any one of the channels can be theoretically estimated through  $C(\theta_S, \theta_{AS}) \propto [(\cos \vartheta + \sin \vartheta) \cos(\theta_S - \theta_{AS}) + (\cos \vartheta - \sin \vartheta) \cos(\theta_S + \theta_{AS})]^2$  [25]. With the parameter  $\vartheta = 0.7 \times (\pi/4)$  calculated above, we calculated the correlation functions and then obtained the highest possible Bell parameter for the single-mode case in our system, which is  $S_{\max} \approx 2.67$ .

As pointed out in previous work [55], although temporally multiplexed QIs storing  $m$  spin waves promise an  $m$ -fold increase in the probability of generating an atom-photon entanglement state compared with single-mode QIs, unwanted spin waves associated with undetected Stokes photons are also created in the temporal-multimode spin-wave memory. These unwanted spin waves are retrieved during the read-out process and emitted in all directions [55], inducing additional noise in the read mode. We now describe this additional noise. The probability of detecting a Stokes photon in one time bin in the  $\text{CH}_\alpha$  channel is written as

$$P_{S_\alpha} = \chi_\alpha \eta_w, \quad (6)$$

where  $\eta_w$  is the detection efficiency of a Stokes photon in the  $\text{CH}_\alpha$  channel. The probability of detecting an anti-Stokes photon retrieved from the temporally multiplexed spin-wave memory storing  $m$  modes in the  $\text{CH}_\alpha$  channel is written

as [73]

$$P_{AS_\alpha}(m) = \chi_\alpha \gamma_\alpha \eta_r + N_s (1 - \gamma_\alpha) \beta_{r,\alpha} \xi_{se} \eta_r + (m-1) N_s \beta_{r,\alpha} \xi_{se} \eta_r, \quad (7)$$

where  $\gamma_\alpha$  is the intrinsic efficiency of the retrieving spin wave in the individual mode in the  $\text{CH}_\alpha$  channel,  $m$  is the spin-wave mode number, which is equal to the number of applied write pulses,  $N_s = \chi_\alpha / \beta_{w,\alpha}$  is the total number of created spin excitations per write pulse in the atomic ensemble [46,73],  $\beta_{w,\alpha}(\beta_{r,\alpha})$  is the fraction of solid angle corresponding to the Stokes (anti-Stokes) photon-collection mode,  $\eta_r$  is the detection efficiency of anti-Stokes photons in the  $\text{CH}_\alpha$  channel, and  $\xi_{se}$  is the branching ratio corresponding to the read photon transition, which is on the order of  $10^{-1}$  in the present experiment.

With  $N_s = \chi_\alpha / \beta_{w,\alpha}$ , we rewrite the probability  $P_{AS_\alpha}(m)$  in Eq. (7) as

$$P_{AS_\alpha}(m) = \chi_\alpha \gamma_\alpha \eta_r + \chi_\alpha (1 - \gamma_\alpha) \frac{\beta_{r,\alpha}}{\beta_{w,\alpha}} \xi_{se} \eta_r + (m-1) \chi_\alpha \frac{\beta_{r,\alpha}}{\beta_{w,\alpha}} \xi_{se} \eta_r. \quad (8)$$

In the above expression, the first term ( $\chi_\alpha \gamma_\alpha \eta_r$ ) denotes the anti-Stokes photon retrieved from the heralded spin wave, the second term denotes the noise due to the imperfect retrieval efficiency, and the last term denotes the additional noise resulting from nondirectional emissions of the unwanted spin waves [55] induced by  $m-1$  write pulses. The probability of detecting a coincidence between the Stokes and anti-Stokes photons in each mode in the  $\text{CH}_\alpha$  channel is written as

$$P_{S_\alpha AS_\alpha}(m) = \chi_\alpha \gamma_\alpha \eta_w \eta_r + P_{S_\alpha} P_{AS_\alpha}(m), \quad (9)$$

where  $P_{S_\alpha} P_{AS_\alpha}(m) = \chi_\alpha^2 \gamma_\alpha \eta_w \eta_r + \chi_\alpha^2 \eta_w (1 - \gamma_\alpha) \frac{\beta_{r,\alpha}}{\beta_{w,\alpha}} \xi_{se} \eta_r + \chi_\alpha^2 \eta_w (m-1) \frac{\beta_{r,\alpha}}{\beta_{w,\alpha}} \xi_{se} \eta_r$  denotes an accidental probability in the coincidence. In this expression, the first and second terms correspond to an accidental event in single-mode memory and the third term corresponds to an accidental event due to the additional noise resulting from the unwanted spin waves with  $m-1$  modes.

For a single-mode atom-photon entangled state, the Bell parameter  $S$  can be measured from the correlation functions and can be expressed as  $S = 2\sqrt{2}V$  [74], where  $V$  denotes the entanglement visibility of the two-photon coincidence, which can be obtained by measuring the interference fringes of the correlation functions as functions of the Stokes phase. In this way, the Bell parameter for the atom-photon entanglement with  $m$  spin-wave storage modes generated in the channel  $\alpha$  can be written as  $S_\alpha(m) = 2\sqrt{2}V_\alpha(m)$ , where  $V_\alpha(m)$  is the visibility of the atom-photon entanglement state. To theoretically evaluate the visibility  $V_\alpha(m)$ , we may express  $V_\alpha(m)$  as  $V_\alpha(m) = V'_\alpha(1) \frac{P_{S_\alpha AS_\alpha}(m) - P_{S_\alpha} P_{AS_\alpha}(m)}{P_{S_\alpha AS_\alpha}(m) + P_{S_\alpha} P_{AS_\alpha}(m)}$ , where the factor  $V'_\alpha(1)$  is less than 1 as a result of the deviation of the parameter  $\cos \vartheta$  from the ideal value of  $1/\sqrt{2}$  and the imperfect phase compensation of the optical elements. The term  $V_\alpha(m) = V'_\alpha(1) \frac{P_{S_\alpha AS_\alpha}(m) - P_{S_\alpha} P_{AS_\alpha}(m)}{P_{S_\alpha AS_\alpha}(m) + P_{S_\alpha} P_{AS_\alpha}(m)}$  describes the decrease in the visibility due to multiphoton errors. (See Fig. 3 for the value of  $V'_\alpha(1)$ .) When  $m=1$ , the term  $V_\alpha(m) = V'_\alpha(1) \frac{P_{S_\alpha AS_\alpha}(m) - P_{S_\alpha} P_{AS_\alpha}(m)}{P_{S_\alpha AS_\alpha}(m) + P_{S_\alpha} P_{AS_\alpha}(m)}$  corresponds to  $\frac{g^{(2)}-1}{g^{(2)}+1}$  and we then have  $V_\alpha(1) = V'_\alpha(1) \frac{g^{(2)}-1}{g^{(2)}+1}$ , where  $g^{(2)} = \frac{P_{S_\alpha AS_\alpha}(m=1)}{P_{S_\alpha}(m=1) P_{AS_\alpha}(m=1)}$  denotes the cross-correlation function. Using the expressions for  $P_{S_\alpha AS_\alpha}(m)$ ,  $P_{S_\alpha}$ , and  $P_{AS_\alpha}(m)$ , we can rewrite the visibility  $V_\alpha(m)$  as

$$V_\alpha(m) \approx \frac{V'_\alpha(1)}{1 + 2(\chi_\alpha + \frac{\chi_\alpha}{\gamma_\alpha} (1 - \gamma_\alpha) \xi_{se} (\beta_{r,\alpha} / \beta_{w,\alpha}))} \cdot \frac{1}{1 + \frac{2(m-1) \chi_\alpha \xi_{se} (\beta_{r,\alpha} / \beta_{w,\alpha})}{\gamma_\alpha} / (1 + 2(\chi_\alpha + \frac{\chi_\alpha}{\gamma_\alpha} (1 - \gamma_\alpha) \xi_{se} (\beta_{r,\alpha} / \beta_{w,\alpha}))}.$$

For the excitation probability  $\chi_\alpha \ll 1$ , we assume that  $\chi_\alpha + \frac{\chi_\alpha}{\gamma_\alpha} (1 - \gamma_\alpha) \xi_{se} (\beta_{r,\alpha} / \beta_{w,\alpha}) \approx 0$ . In this case, we have

$$V_\alpha(m) = \frac{V'_\alpha(1)}{1 + 2\chi_\alpha (m-1) \xi_{se} (\beta_{r,\alpha} / \beta_{w,\alpha}) / \gamma_\alpha}. \quad (10)$$

The Bell parameter can be evaluated as

$$S_\alpha(m) = 2\sqrt{2}V_\alpha(m) = \frac{2\sqrt{2}V'_\alpha(1)}{1 + 2\chi_\alpha (m-1) \xi_{se} (\beta_{r,\alpha} / \beta_{w,\alpha}) / \gamma_\alpha}. \quad (11)$$

Equations (10) and (11) show that the visibility and Bell parameters of the temporally multiplexed atom-photon entanglement decrease with the mode number  $m$ . For  $m=1$ ,  $V_\alpha(1) \approx V'_\alpha(1)$ , which means that  $\frac{g^{(2)}-1}{g^{(2)}+1} \approx 1$ . Therefore, Eqs. (10) and (11) are reasonable only for cases in which  $g^{(2)}$  is high, i.e.,  $\chi_\alpha \ll 1$ , as mentioned above.

In previous experiments on atom-photon entanglement [21–24,55], the collection of write and read photons was symmetric, i.e.,  $\beta_{r,\alpha} / \beta_{w,\alpha} \approx 1$ . For suppressing the additional

noise in the temporal-multimode spin-wave memory, we set up the asymmetric photon-collection channel  $\text{CH}_1$ , where we expect that  $\beta_{r,\alpha} / \beta_{w,\alpha} < 1$ . To explain how the asymmetric photon-collection channel gives  $\beta_{r,\alpha} / \beta_{w,\alpha} < 1$ , we evaluate the ratios  $\beta_{r,\alpha} / \beta_{w,\alpha}$  for the asymmetric and symmetric photon-collection channels. When a write laser pulse is applied to an atomic ensemble along a particular direction, for example, the  $x$  axis in our experiment, it induces spontaneous emission of the Stokes photons and simultaneously creates a DLCZ memory (spin wave). The Stokes photons randomly emit in various directions, i.e., over a  $4\pi$  solid angle. For simplicity, we assume that the Stokes photons emit in a spherical-wave mode, with the emission center being the center of the atoms. The optical collection areas of the fiber collimators  $\text{FC}_{S1}$  and  $\text{FC}_{S2}$  can be evaluated as  $A_{w,1} = \frac{\pi(d_{w,1})^2}{4}$  and  $A_{w,2} = \frac{\pi(d_{w,2})^2}{4}$ , where  $d_{w,1}$  and  $d_{w,2}$  are the diameters of  $\text{FC}_{S1}$  and  $\text{FC}_{S2}$ , respectively. As shown in Figs. 1(b) and 1(c),  $\text{FC}_{S1}$  and  $\text{FC}_{S2}$  are both located at the position  $x_1 = -1.2$  m. The solid angles of the Stokes photons collected in  $\text{CH}_1$  and  $\text{CH}_2$  can be estimated as  $\Omega_{w,1} = \frac{A_{w,1}}{(x_1 - x_0)^2}$  and  $\Omega_{w,2} = \frac{A_{w,2}}{(x_1 - x_0)^2}$ ,

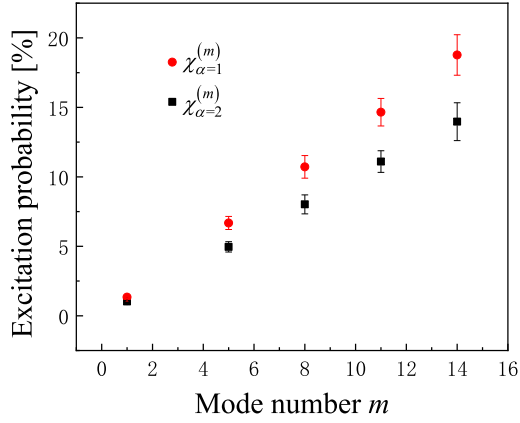


FIG. 2. Measured excitation probabilities  $\chi_{\alpha=1}^{(m)}$  (red circles) and  $\chi_{\alpha=2}^{(m)}$  (black squares) as a function of mode number  $m$  for the write beam with  $100 \mu\text{W}$  power. Error bars in the experimental data represent 1 standard deviation, which is estimated from the Poissonian detection statistics.

respectively, where  $x_0 = 0$  denotes the coordinate value of the center of the atoms. The heralded spin-wave memories are mapped into read-out (anti-Stokes) photons by applying the read laser pulse. In the read process, the unwanted spin waves mentioned in Eq. (8) are also retrieved, mapped into noise photons, and emitted in all directions, i.e., over a  $4\pi$  solid angle. The solid angles of the read-out photon noise collected by the fiber collimators  $\text{FC}_{\text{AS1}}$  and  $\text{FC}_{\text{AS2}}$  in  $\text{CH}_1$  and  $\text{CH}_2$  are estimated as  $\Omega_{r,1} = \frac{A_{r,1}}{(x_2 - x_0)^2} = \frac{\pi}{4} \left( \frac{d_{r,1}}{x_2 - x_0} \right)^2$  and  $\Omega_{r,2} = \frac{A_{r,2}}{(x_2 - x_0)^2} = \frac{\pi}{4} \left( \frac{d_{r,2}}{x_2 - x_0} \right)^2$ , where  $x_2 = 1250 \text{ mm}$  denotes the position of  $\text{FC}_{\text{AS1}}$  ( $\text{FC}_{\text{AS2}}$ ) along the  $x$  axis, and  $d_{r,1}$  and  $d_{r,2}$  denote the diameters of  $\text{FC}_{\text{AS2}}$  and  $\text{FC}_{\text{AS1}}$ , respectively, which were provided above. In the  $\text{CH}_\alpha$  channel ( $\alpha = 1, 2$ ), the fractions of the solid angles, which were defined in Eq. (7), can be expressed as  $\beta_{w,\alpha} = \Omega_{w,\alpha}/4\pi$  for the Stokes photon collection and  $\beta_{r,\alpha} = \Omega_{r,\alpha}/4\pi$  for the anti-Stokes photon collection, respectively. Since the difference between the separation distances  $|x_1 - x_0|$  and  $|x_2 - x_0|$  is small, we assume that  $|x_1 - x_0| \approx |x_2 - x_0|$  in the following estimate. The ratio of the solid angle fraction for collecting Stokes photons to that for collecting read-out (anti-Stokes) photons can be estimated as  $r_1 = \frac{\beta_{w,1}}{\beta_{r,1}} = \frac{A_{w,1}}{A_{r,1}}$  for the asymmetrical channel ( $\text{CH}_1$ ) and  $r_2 = \frac{\beta_{w,2}}{\beta_{r,2}} = \frac{A_{w,2}}{A_{r,2}}$  for the symmetrical channel ( $\text{CH}_2$ ). As discussed above, the diameters of the collimators  $\text{FC}_{\text{S1}}$ ,  $\text{FC}_{\text{AS1}}$ ,  $\text{FC}_{\text{S2}}$ , and  $\text{FC}_{\text{AS2}}$  are 2.6, 1.2, 1.3, and 1.3 mm, respectively, and thus, we have  $r_1 \approx 4.69$  and  $r_2 \approx 1$ .

### III. EXPERIMENTAL RESULTS AND ANALYSIS

By applying a train containing  $m$  write laser pulses with each pulse coming from a different direction to a cloud of cold atoms, we generate atom-photon (photon-photon) entanglement in  $m$  temporal modes.

The red circles and black squares in Fig. 2 are the measured generation probabilities  $\chi_{\alpha=1}^{(m)}$  and  $\chi_{\alpha=2}^{(m)}$  as a function of the mode number  $m$  for the case that each write pulse has a power

of  $100 \mu\text{W}$ . The measured results show that the probabilities  $\chi_{\alpha=1}^{(m)}$  and  $\chi_{\alpha=2}^{(m)}$  increase linearly with  $m$ , i.e., that the QI storing  $m$  spin-wave modes may increase the probability of generating atom-photon entanglement by a factor of  $m$ . On the other hand, the atom-photon entanglement excitation probability ( $\chi_{\alpha=1}^{(m)}$ ) in  $\text{CH}_1$  is significantly larger than that in  $\text{CH}_2$  ( $\chi_{\alpha=2}^{(m)}$ ). The reason for this is that the Stokes collection angle in the  $\text{CH}_1$  channel is larger than that in  $\text{CH}_2$ .

In the following coincidence measurements of the two photons, the excitation probabilities  $\chi_{\alpha=1}$  and  $\chi_{\alpha=2}$  are both set to be  $\sim 1\%$ , as obtained by choosing the powers of the individual write pulses to be 75 and  $100 \mu\text{W}$ , respectively.

We measure the retrieval efficiencies of the spin waves  $M(t_1), M(t_2) \dots M(t_{m=14})$  in the  $\text{CH}_1$  ( $\text{CH}_2$ ) channel and find that they are basically similar. The average retrieval efficiency in the  $\text{CH}_1$  channel is  $\gamma_1 = 15.8(\pm 0.5)\%$  and that in  $\text{CH}_2$  is  $\gamma_2 = 16.7(\pm 0.6)\%$ . The retrieval efficiency in the asymmetrical channel ( $\text{CH}_1$ ) is slightly less than that in the symmetrical channel ( $\text{CH}_2$ ). In the following, we explain the slightly different retrieval efficiencies. In our present experiment, a spin wave paired with a Stokes photon can be randomly created by a write laser pulse. If the Stokes photon is detected, the creation of the spin wave is heralded. A read laser beam will then be applied along the direction opposite to the write pulse to retrieve the heralded spin wave. According to the phase-matched condition, the read-out photon propagates along the direction opposite to that of the Stokes photon and is then collected by fiber collimators. For the asymmetrical channel, the beam mode of the write-out photon is different from that of read-out photons in the atomic ensemble, which results in a phase mismatch in their wave vectors. In addition, the effective interaction area of the atoms is different for the write-read process. However, since the divergence angles ( $\lambda/\pi\omega$ ) of the laser beams ( $\omega \sim 500 \mu\text{m}$ ) are very small ( $\sim 5 \times 10^{-4}$ ), the phase mismatch has a small effect on the retrieval efficiency. Therefore, the asymmetrical channel gives rise to a slight decrease in the retrieval efficiency.

The red circles and blue squares in Fig. 3 show the measured  $S_{\alpha=1}^{(m)}$  and  $S_{\alpha=2}^{(m)}$  data when the memory stores  $m$  modes. For  $m = 1$ , the measured Bell parameter for the two channels is  $S \approx 2.58$ , which is less than the theoretically expected value of  $S \approx 2.67$ . We attribute this difference mainly to the imperfect optical phase compensation in our experimental setup. In Fig. 3, the measured Bell parameters  $S_{\alpha=1}^{(m=14)}$  and  $S_{\alpha=2}^{(m=14)}$  are  $2.36 \pm 0.03$  and  $2.24 \pm 0.04$ , respectively, showing that the asymmetrical configuration increases the Bell parameter  $S$  by 0.12 compared with the symmetrical configuration. According to the relationship  $S_{\text{exp}} = 2\sqrt{2}V$ , we evaluated the visibilities for the asymmetric and symmetric channels to be  $V \approx 0.834$  and  $V \approx 0.792$ , respectively. With the expression  $F = \frac{3V+1}{4}$  [75], we obtain entanglement fidelities of  $F \approx 87.6\%$  and  $F \approx 84.4\%$  for the asymmetric and symmetric photon-collection channels, respectively, which show that the QI using the asymmetric channel increases the entanglement fidelity by  $\sim 3\%$ . The red dashed (blue solid) line in Fig. 3 is the fit to the experimental data of  $\text{CH}_1$  ( $\text{CH}_2$ ) based on Eq. (11), which gives  $r_1 = \frac{\beta_{w,1}}{\beta_{r,1}} \approx 1.7$  ( $r_2 = \frac{\beta_{w,2}}{\beta_{r,2}} \approx 1$ ) for the asymmetric (symmetric) channel. The fitted result  $r_1 \approx 1.7$

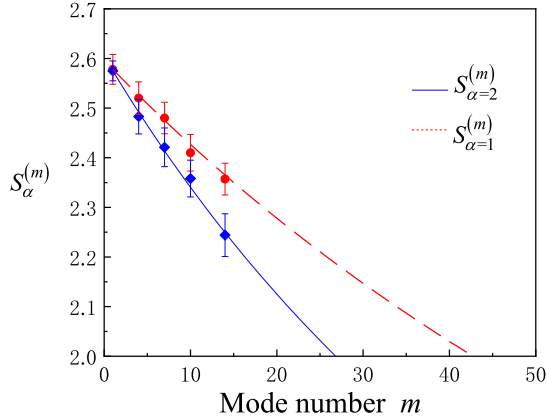


FIG. 3. Measured Bell parameter  $S_{\alpha=1}^{(m)}$  (red circles)  $S_{\alpha=2}^{(m)}$  (blue squares) as a function of mode number  $m$  for the excitation probabilities  $\chi_{\alpha=1} \approx 1\%$  and  $\chi_{\alpha=2} \approx 1\%$ . The red dashed and blue solid curves are the fittings by using Eq. (11). In the fittings, branching ratio  $\xi_{se}=0.093$ , retrieval efficiencies  $\gamma_{\alpha=1} = 15.8\%$  and  $\gamma_{\alpha=2} = 16.7\%$ , the ratios of the solid angles  $r_1 \approx 1.7(\beta_{r,\alpha=1}/\beta_{w,\alpha=1} \approx 1/1.7)$  and  $r_2 = 1(\beta_{r,\alpha=2}/\beta_{w,\alpha=2} \approx 1)$ , the visibilities for single-mode  $V_{\alpha=1}(1) \approx V'_{\alpha=2}(1) \approx 0.91$ . Error bars in the experimental data represent 1 standard deviation, which is estimated from the Poissonian detection statistics.

is far lower than the estimated result of  $r_1 \approx 4.69$ . We attribute this discrepancy to the following two causes: (1) In our spherical-wave mode, the interactions between the write-read laser beam and the atoms are assumed to occur at the center of the atoms. In reality, the interactions occur in the overlapping area between the write-read laser beam and the atoms. (2) In our estimation of the solid angles, we assume that the fiber collimators can effectively collect the spherical-wave mode of photon emissions. In reality, the collimators can effectively collect the TEM00 laser mode. We expect that future work could lead to the development of a complex model to describe our experimental results well and further improve the repeater performance.

Based on the fits in Fig. 3, one may expect that when satisfying violations of the Bell inequality, the multiplexed QI using the asymmetrical channel can store 42 modes, while the multiplexed QI using a symmetrical channel can store 26 modes.

To investigate the multimode storage ability of the ensemble, we measure the decay of the Bell parameter  $S_{\alpha=1}^{(m=14)}$  and  $S_{\alpha=2}^{(m=14)}$  with the storage time  $t$  for the generation probabilities  $\chi_{\alpha=1} \approx \chi_{\alpha=2} \approx 1\%$ , respectively. The red circles (black squares) in Fig. 4 depict the measured  $S_{\alpha}^{(m=14)}$  as a function of the storage time  $t$ . In the CH<sub>1</sub> channel, the measured Bell parameter  $S_{\alpha=1}^{(m=14)} = 2.12 \pm 0.04$  for the storage time  $t = 25 \mu\text{s}$  violates the Bell inequality by 3 standard deviations. In the CH<sub>2</sub> channel, the measured  $S_{\alpha=2}^{(m=14)} = 2.06 \pm 0.03$  for the storage time  $t = 20 \mu\text{s}$  violates the Bell inequality by 2 standard deviations. Since the errors on the  $S_{\alpha=1}^{(m=14)}$  data are comparable with those on the  $S_{\alpha=2}^{(m=14)}$  data, the stability associated with generating multimode atom-photon entanglement in CH<sub>2</sub> is basically the same as that in CH<sub>1</sub>.

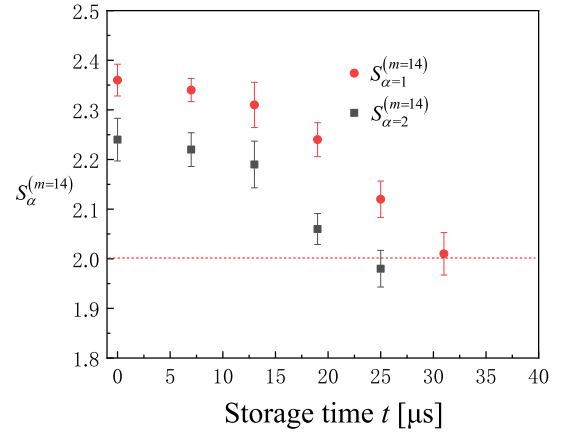


FIG. 4. Bell parameter  $S_{\alpha=1}^{(m=14)}$  ( $S_{\alpha=2}^{(m=14)}$ ) as a function of storage time  $t$  for the excitation probability  $\chi_{\alpha=1} \approx 1\%$  ( $\chi_{\alpha=2} \approx 1\%$ ). The red circles (black squares) depict the measured  $S_{\alpha}^{(m=14)}$  for various storage times  $t$  in CH <sub>$\alpha$</sub>  channel. Error bars in the experimental data represent 1 standard deviation, which is estimated from the Poissonian detection statistics.

#### IV. DISCUSSION AND CONCLUSION

We have experimentally demonstrated a scheme that can improve the entanglement quality of temporal multimode atom-photon QIs by using an asymmetric photon-collection channel instead of a symmetric one. When the atom-photon entanglement QIs store 14 temporal modes, the measured Bell parameters  $S$  are  $2.24 \pm 0.04$  and  $2.36 \pm 0.03$  for QIs using symmetrical and asymmetrical channels, respectively, showing that the QIs using asymmetric channels give rise to a 3% increase in entanglement fidelity over QIs using symmetric channels. The physics behind this entanglement improvement can be explained as follows. For temporal multimode atom-photon QIs, the additional noise is proportional to the ratio  $\beta_r/\beta_w(1/t)$  [46]. Since the ratio  $\beta_r/\beta_w$  in a temporal-multimode atom-photon QI that uses an asymmetric photon-collection channel is smaller than that in one that uses a symmetric photon-collection channel, the visibility of atom-photon entanglement for a QI using an asymmetric photon-collection channel is better. Based on the fits in Fig. 3, the storage temporal mode number in a multiplexed QI using the asymmetrical channel promising to violate the Bell inequality is expected to be up to 42, which is far beyond the value of 26 modes for the multiplexed QI using a symmetrical one. In contrast to the cavity-enhanced noise-suppression scheme in Ref. [73], our asymmetric photon-collection scheme promises cavity-enhanced readout. The presented temporal multimode DLCZ-like memories can be combined with the spatial multiplexing scheme [43] to achieve large-scale multiplexed QIs. Considering a multiplexed atom-photon entanglement source that stores 14 temporal and 15 spatial SW qubits, the total number of memory qubits will reach  $N_m = 14 \times 15 = 210$ . Moreover, the presented temporally multiplexed scheme allows one to improve the retrieval efficiency via cavity-enhanced atom-photon coupling.

In our experiment, the measured Bell parameter for single-mode spin-wave-photon entanglement in the sym-

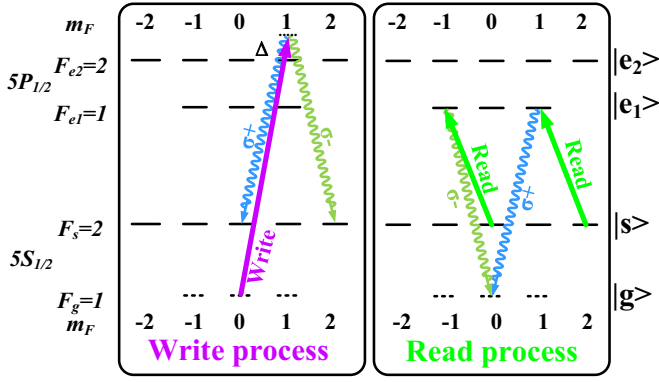


FIG. 5. Relevant atomic levels for the proposed scheme.

metric and asymmetric channels is  $S \approx 2.58$ , which is lower than the ideal Bell parameter value of  $2\sqrt{2}$ . A main limitation to the measured results is that the highest possible Bell parameter in our presented scheme is  $S_{\max} \approx 2.67$ . To improve the maximum Bell parameter value, we propose a scheme. In this scheme, the atomic memory still uses cold  $^{87}\text{Rb}$  atoms. The relevant atomic levels  $|g\rangle = |5S_{1/2}, F_g = 1\rangle$ ,  $|s\rangle = |5S_{1/2}, F_s = 2\rangle$ ,  $|e_1\rangle = |5P_{1/2}, F_{e1} = 1\rangle$ , and  $|e_2\rangle = |5P_{1/2}, F_{e2} = 2\rangle$  are shown in Fig. 5.

In contrast to the presented experiment, the atoms are initially prepared in the Zeeman level  $|g, m_g = 0\rangle$  via optical pumping, where  $m_g$  denotes the magnetic quantum number of  $|g\rangle$ . A right-circularly polarized write pulse with a frequency blue detuned from the  $|g\rangle \rightarrow |e_2\rangle$  transition by 20 MHz is applied. The write pulse will induce Raman transitions  $|g, m_g = 0\rangle \rightarrow |s, m_s = 2\rangle$  ( $|g, m_g = 0\rangle \rightarrow |s, m_s = 0\rangle$ ) via  $|e_2, m_{e2} = 1\rangle$ , which emits a right-circularly polarized (left-circularly polarized) Stokes photon and simultaneously creates a spin-wave excitation associated with the coherence  $|g, m_g = 0\rangle \leftrightarrow |s, m_s = 0\rangle$  ( $|g, m_g = 0\rangle \leftrightarrow |s, m_s = 2\rangle$ ). The above Raman processes will create an atom-photon entanglement state, written as  $|\Phi_{ap}\rangle = \cos\vartheta |R\rangle |S_{00}\rangle + \sin\vartheta |S_{02}\rangle$ , where  $|R\rangle(|L\rangle)$  denotes a right- (left-) circularly polarized Stokes photon,  $|S_{00}\rangle(|S_{02}\rangle)$  denotes one spin-wave excitation associated with the Zeeman coherence  $|g, m_g = 0\rangle \leftrightarrow |s, m_s = 0\rangle$  ( $|g, m_g = 0\rangle \leftrightarrow |s, m_s = 2\rangle$ ), the parameter  $\vartheta$  can be obtained according to  $\cos^2\vartheta = X_{m_g=0}^2(\mu=1)/(X_{m_g=0}^2(\mu=1) + X_{m_g=0}^2(\mu=-1))$ , where  $X_{m_g=0}(\mu) = C_{m_g=0, \mu_w=1, m_F+\mu_w=1}^{F_g, 1, F_{e2}} C_{m_g+\mu_w=1, \mu, m_g+\mu_w+\mu}^{F_{e2}, 1, F_s}$  is the product of the relevant Clebsch-Gordan coefficients for the transitions,  $\mu_w = 1$  is the helicity of the write laser field, and  $\mu = +1(-1)$  is the right- (left-) circularly polarized Stokes photon. Based on the Clebsch-Gordan coefficients for the write-laser transition  $|g\rangle \rightarrow |e_2\rangle$  ( $|5S_{1/2}, F_g = 1\rangle \rightarrow |5P_{1/2}, F_{e2} = 2\rangle$ ) and write-out photon transition  $|e_2\rangle \rightarrow |s\rangle$  ( $|5P_{1/2}, F_{e2} = 2\rangle \rightarrow |5S_{1/2}, F_s = 2\rangle$ ), we obtain  $\cos\vartheta = \sqrt{3/5}$ , which corresponds to  $\vartheta = 0.87 \times (\pi/4)$ . By applying a left-circularly polarized read pulse with its frequency tuned to the  $|s\rangle \rightarrow |e_1\rangle$  transition, the spin-wave-photon entanglement can be mapped into two-photon entanglement (see the read process in Fig. 5). The highest possible Bell parameter can be theoretically evaluated from the coincidence expression  $C(\theta_S, \theta_{AS}) \propto$

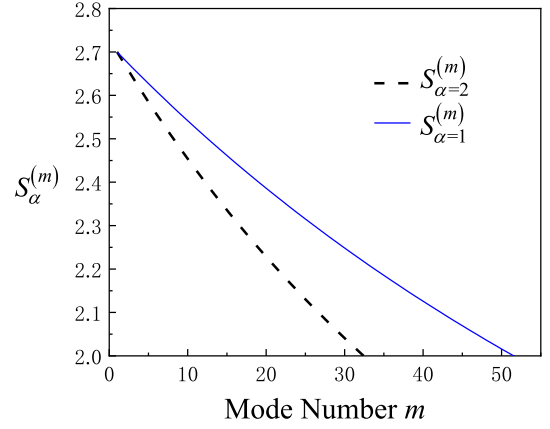


FIG. 6. Expected results of Bell parameters  $S_{\alpha=1}^{(m)}$  (blue solid curve) and  $S_{\alpha=2}^{(m)}$  (black dashed curve) as a function of mode number  $m$  for the proposed scheme with  $V_{\alpha=1}(1) \approx V'_{\alpha=2}(1) \approx 0.95$ . The other parameters are the same as those in Fig. 3.

$[(\cos\vartheta + \sin\vartheta)\cos(\theta_S - \theta_{AS}) + (\cos\vartheta - \sin\vartheta)\cos(\theta_S + \theta_{AS})]^2$  mentioned above. Based on it, we calculated the correlation functions and then obtained the highest possible Bell parameter of  $S'_{\max} \approx 2.8$  for the proposed scheme. Compared to the presented scheme, the proposed scheme may increase the maximum Bell parameter by a factor of  $F \approx S'_{\max}/S_{\max} \approx 2.8/2.67 \approx 1.05$ . When using the proposed scheme instead of the presented scheme, the measured Bell parameter (visibility) for the single-mode ( $m = 1$ ) spin-wave-photon entanglement may be increased by the same factor  $F \approx 1.05$  and then reaches  $S \approx 2.7(V'(1) \approx S/2\sqrt{2} \approx 0.95)$ . In this case, we theoretically calculated Bell parameters  $S_{\alpha=1}^{(m)}$  (blue solid curve) for the asymmetric channel and  $S_{\alpha=2}^{(m)}$  (black dashed curve) for the symmetrical channel as a function of the mode number  $m$  according to Eq. (11). The results are presented in Fig. 6, and show that, when satisfying violations of the Bell inequality, the multiplexed QI using the asymmetrical channel can be expected to store 51 modes, while the multiplexed QI using the symmetrical channel only stores 32 modes.

The short storage lifetime ( $\sim 25 \mu\text{s}$ ) can be extended by trapping atoms in an optical lattice [15,17] and selecting two magnetic field insensitive spin waves to store memory qubits [76,77]. To minimize transmission losses in fibers, one can convert the Stokes photons (795 nm) into photons in the telecommunications band [78–80]. Since the temporal-multimode Stokes photons propagate in a spatial channel, the conversion is done in a waveguide device. The presented work paves the road to achieving high-performance QIs and will benefit QR-based long-distance quantum communications.

## ACKNOWLEDGMENTS

We acknowledge funding support from Key Project of the Ministry of Science and Technology of China (Grant No. 2016YFA0301402); The National Natural Science Foundation of China (Grants No. 11475109 and No. 11974228). Fund for Shanxi Grant No. “1331 Project” Key Subjects Construction.

- [1] H. J. Kimble, The quantum internet, *Nature (London)* **453**, 7198 (2008).
- [2] S. Wehner, D. Elkouss, and R. Hanson, D. Elkouss, and R. Hanson, Quantum internet: A vision for the road ahead, *Science* **362**, 6412 (2018).
- [3] C. Simon, Towards a global quantum network, *Nat. Photonics* **11**, 678 (2017).
- [4] N. Sangouard, C. Simon, H. de Riedmatten, and N. Gisin, Quantum repeaters based on atomic ensembles and linear optics, *Rev. Mod. Phys.* **83**, 33 (2011).
- [5] L.-M. Duan, M. D. Lukin, J. I. Cirac, and P. Zoller, Long-distance quantum communication with atomic ensembles and linear optics, *Nature (London)* **414**, 22 (2001).
- [6] H.-J. Briegel, W. Dür, J. I. Cirac, and A. P. Zoller, Quantum Repeaters: The Role of Imperfect Local Operations in Quantum Communication, *Phys. Rev. Lett.* **81**, 5932 (1998).
- [7] A. Kuzmich, W. P. Bowen, A. D. Boozer, A. Boca, C. W. Chou, L.-M. Duan, and H. J. Kimble, Generation of nonclassical photon pairs for scalable quantum communication with atomic ensembles, *Nature (London)* **423**, 731 (2003).
- [8] C. W. Chou, H. de Riedmatten, D. Felinto, S. V. Polyakov, S. J. van Enk, and H. J. Kimble, Measurement-induced entanglement for excitation stored in remote atomic ensembles, *Nature (London)* **438**, 7069 (2005).
- [9] J. Laurat, H. de Riedmatten, D. Felinto, C.-W. Chou, E. W. Schomburg, and H. J. Kimble, Efficient retrieval of a single excitation stored in an atomic ensemble, *Opt. Express* **14**, 15 (2006).
- [10] J. Simon, H. Tanji, J. K. Thompson, and V. Vuletic, Interfacing Collective Atomic Excitations and Single Photons, *Phys. Rev. Lett.* **98**, 183601 (2007).
- [11] D. Felinto, C. W. Chou, H. de Riedmatten, S. V. Polyakov, and H. J. Kimble, Control of decoherence in the generation of photon pairs from atomic ensembles, *Phys. Rev. A* **72**, 053809 (2005).
- [12] J. Laurat, K. S. Choi, H. Deng, C. W. Chou, and H. J. Kimble, Heralded Entanglement between Atomic Ensembles: Preparation, Decoherence, and Scaling, *Phys. Rev. Lett.* **99**, 180504 (2007).
- [13] B. Zhao, Y.-A. Chen, X.-H. Bao, T. Strassel, C.-S. Chuu, X.-M. Jin, J. Schmiedmayer, Z.-S. Yuan, S. Chen, and J.-W. Pan, A millisecond quantum memory for scalable quantum networks, *Nat. Phys.* **5**, 95 (2009).
- [14] X.-H. Bao, A. Reingruber, P. Dietrich, J. Rui, A. Dück, T. Strassel, L. Li, N.-L. Liu, B. Zhao, and J.-W. Pan, Efficient and long-lived quantum memory with cold atoms inside a ring cavity, *Nat. Phys.* **8**, 517 (2012).
- [15] R. Zhao, Y. O. Dudin, S. D. Jenkins, C. J. Campbell, D. N. Matsukevich, T. A. B. Kennedy, and A. Kuzmich, Long-lived quantum memory, *Nat. Phys.* **5**, 100 (2009).
- [16] A. G. Radnaev, Y. O. Dudin, R. Zhao, H. H. Jen, S. D. Jenkins, A. Kuzmich, and T. A. B. Kennedy, A quantum memory with telecom-wavelength conversion, *Nat. Phys.* **6**, 11 (2010).
- [17] S.-J. Yang, X.-J. Wang, X.-H. Bao, and J.-W. Pan, An efficient quantum light-matter interface with sub-second lifetime, *Nat. Photonics* **10**, 381 (2016).
- [18] X.-L. Pang, A.-L. Yang, J.-P. Dou, H. Li, C.-N. Zhang, E. Poem, D. J. Saunders, H. Tang, J. Nunn, I. A. Walmsley, and X.-M. Jin, A hybrid quantum memory-enabled network at room temperature, *Sci. Adv.* **6**, 1425 (2020).
- [19] M. Zugenmaier, K. B. Dideriksen, A. S. Sørensen, B. Albrecht, and E. S. Polzik, Long-lived non-classical correlations towards quantum communication at room temperature, *Commun. Phys.* **1**, 76 (2018).
- [20] K. B. Dideriksen, R. Schmieg, M. Zugenmaier, and E. S. Polzik, Room-temperature single-photon source with near-millisecond built-in memory, *Nat. Commun.* **12**, 3699 (2021).
- [21] D. N. Matsukevich and A. Kuzmich, Quantum state transfer between matter and light, *Science* **306**, 5696 (2004).
- [22] H. de Riedmatten, J. Laurat, C. W. Chou, E. W. Schomburg, D. Felinto, and H. J. Kimble, Direct Measurement of Decoherence for Entanglement between a Photon and Stored Atomic Excitation, *Phys. Rev. Lett.* **97**, 113603 (2006).
- [23] S. Chen, Y. A. Chen, B. Zhao, Z. S. Yuan, J. Schmiedmayer, and J. W. Pan, Demonstration of a Stable Atom-Photon Entanglement Source for Quantum Repeaters, *Phys. Rev. Lett.* **99**, 180505 (2007).
- [24] K. Kutluer, E. Distante, B. Casabone, S. Duranti, M. Mazzer, and H. de Riedmatten, Time Entanglement between a Photon and a Spin Wave in a Multimode Solid-State Quantum Memory, *Phys. Rev. Lett.* **123**, 030501 (2019).
- [25] D. N. Matsukevich, T. Chaneliere, M. Bhattacharya, S. Y. Lan, S. D. Jenkins, T. A. Kennedy, and A. Kuzmich, Entanglement of a Photon and a Collective Atomic Excitation, *Phys. Rev. Lett.* **95**, 040405 (2005).
- [26] Y. O. Dudin, A. G. Radnaev, R. Zhao, J. Z. Blumoff, T. A. Kennedy, and A. Kuzmich, Entanglement of Light-Shift Compensated Atomic Spin Waves with Telecom Light, *Phys. Rev. Lett.* **105**, 260502 (2010).
- [27] S. J. Yang, X. J. Wang, J. R. J. Li, X. H. Bao, and J. W. Pan, Highly Retrievable Spin-Wave-Photon Entanglement Source, *Phys. Rev. Lett.* **114**, 210501 (2015).
- [28] D.-S. Ding, W. Zhang, Z.-Y. Zhou, S. Shi, B.-S. Shi, and G.-C. Guo, Raman quantum memory of photonic polarized entanglement, *Nat. Photonics* **9**, 332 (2015).
- [29] Y. Wu, L. Tian, Z. Xu, W. Ge, L. Chen, S. Li, H. Yuan, Y. Wen, H. Wang, C. Xie, and K. Peng, Simultaneous generation of two spin-wave-photon entangled states in an atomic ensemble, *Phys. Rev. A* **93**, 052327 (2016).
- [30] P. Farrera, G. Heinze, and H. de Riedmatten, Entanglement between a Photonic Time-Bin Qubit and a Collective Atomic Spin Excitation, *Phys. Rev. Lett.* **120**, 100501 (2018).
- [31] Y. Mei, Y. Zhou, S. Zhang, J. Li, K. Liao, H. Yan, S. L. Zhu, and S. Du, Einstein-Podolsky-Rosen Energy-Time Entanglement of Narrow-Band Biphotons, *Phys. Rev. Lett.* **124**, 010509 (2020).
- [32] B. Zhao, Z. B. Chen, Y. A. Chen, J. Schmiedmayer, and J. W. Pan, Robust Creation of Entanglement between Remote Memory Qubits, *Phys. Rev. Lett.* **98**, 240502 (2007).
- [33] Z.-B. Chen, B. Zhao, Y.-A. Chen, J. Schmiedmayer, and J.-W. Pan, Fault-tolerant quantum repeater with atomic ensembles and linear optics, *Phys. Rev. A* **76**, 022329 (2007).
- [34] E. Saglamyurek, N. Sinclair, J. Jin, J. A. Slater, D. Oblak, F. Bussières, M. George, R. Ricken, W. Sohler, and W. Tittel, Broadband waveguide quantum memory for entangled photons, *Nature (London)* **469**, 512 (2011).
- [35] C. Clausen, I. Usmani, F. Bussières, N. Sangouard, M. Afzelius, H. de Riedmatten, and N. Gisin, Quantum storage of photonic entanglement in a crystal, *Nature (London)* **469**, 508 (2011).
- [36] E. Saglamyurek, J. Jin, V. B. Verma, M. D. Shaw, F. Marsili, S. W. Nam, D. Oblak, and W. Tittel, Quantum storage of entangled

- telecom-wavelength photons in an erbium-doped optical fibre, *Nat. Photonics* **9**, 83 (2015).
- [37] Y.-A. Chen, S. Chen, Z.-S. Yuan, B. Zhao, C.-S. Chuu, J. Schmiedmayer, and J.-W. Pan, Memory-built-in quantum teleportation with photonic and atomic qubits, *Nat. Phys.* **4**, 103 (2008).
- [38] F. Bussi eres, C. Clausen, A. Tiranov, B. Korzh, V. B. Verma, S. W. Nam, F. Marsili, A. Ferrier, P. Goldner, H. Herrmann, C. Silberhorn, W. Sohler, M. Afzelius, and N. Gisin, Quantum teleportation from a telecom-wavelength photon to a solid-state quantum memory, *Nat. Photonics* **8**, 775 (2014).
- [39] X. H. Bao, X. F. Xu, C. M. Li, Z. S. Yuan, C. Y. Lu, and J. W. Pan, Quantum teleportation between remote atomic-ensemble quantum memories, *Proc. Natl. Acad. Sci. USA* **109**, 50 (2012).
- [40] Z. S. Yuan, Y. A. Chen, B. Zhao, S. Chen, J. Schmiedmayer, and J. W. Pan, Experimental demonstration of a BDCZ quantum repeater node, *Nature (London)* **454**, 7208 (2008).
- [41] Y. Yu, F. Ma, X. Y. Luo, B. Jing, P. F. Sun, R. Z. Fang, C. W. Yang, H. Liu, M. Y. Zheng, X. P. Xie, W. J. Zhang, L. X. You, Z. Wang, T. Y. Chen, Q. Zhang, X. H. Bao, and J. W. Pan, Entanglement of two quantum memories via fibres over dozens of kilometres, *Nature (London)* **578**, 7794 (2020).
- [42] L. Jiang, J. M. Taylor, and M. D. Lukin, Fast and robust approach to long-distance quantum communication with atomic ensembles, *Phys. Rev. A* **76**, 012301 (2007).
- [43] N. Sangouard, C. Simon, B. Zhao, Y.-A. Chen, H. de Riedmatten, J.-W. Pan, and N. Gisin, Robust and efficient quantum repeaters with atomic ensembles and linear optics, *Phys. Rev. A* **77**, 062301 (2008).
- [44] C. Simon, H. de Riedmatten, M. Afzelius, N. Sangouard, H. Zbinden, and N. Gisin, Quantum Repeaters with Photon Pair Sources and Multimode Memories, *Phys. Rev. Lett.* **98**, 190503 (2007).
- [45] O. A. Collins, S. D. Jenkins, A. Kuzmich, and T. A. Kennedy, Multiplexed Memory-Insensitive Quantum Repeaters, *Phys. Rev. Lett.* **98**, 060502 (2007).
- [46] C. Simon, H. de Riedmatten, and M. Afzelius, Temporally multiplexed quantum repeaters with atomic gases, *Phys. Rev. A* **82**, 010304(R) (2010).
- [47] N. Sinclair, E. Saglamyurek, H. Mallahzadeh, J. A. Slater, M. George, R. Ricken, M. P. Hedges, D. Oblak, C. Simon, W. Sohler, and W. Tittel, Spectral Multiplexing for Scalable Quantum Photonics Using an Atomic Frequency Comb Quantum Memory and Feed-Forward Control, *Phys. Rev. Lett.* **113**, 053603 (2014).
- [48] L. Tian, Z. Xu, L. Chen, W. Ge, H. Yuan, Y. Wen, S. Wang, S. Li, and H. Wang, Spatial Multiplexing of Atom-Photon Entanglement Sources Using Feedforward Control and Switching Networks, *Phys. Rev. Lett.* **119**, 130505 (2017).
- [49] M. Bonarota, J. L. Le Gou et, and T. Chaneli ere, Highly multimode storage in a crystal, *New J. Phys.* **13**, 013013 (2011).
- [50] M. Hosseini, B. M. Sparkes, G. Campbell, P. K. Lam, and B. C. Buchler, High efficiency coherent optical memory with warm rubidium vapour, *Nat. Commun.* **2**, 174 (2011).
- [51] M. Hosseini, B. M. Sparkes, G. Hetet, J. J. Longdell, P. K. Lam, and B. C. Buchler, Coherent optical pulse sequencer for quantum applications, *Nature (London)* **461**, 7261 (2009).
- [52] C. Laplane, P. Jobez, J. Etesse, N. Timoney, N. Gisin, and M. Afzelius, Multiplexed on-demand storage of polarization qubits in a crystal, *New J. Phys.* **18**, 013006 (2015).
- [53] I. Usmani, M. Afzelius, H. de Riedmatten, and N. Gisin, Mapping multiple photonic qubits into and out of one solid-state atomic ensemble, *Nat. Commun.* **1**, 1010 (2010).
- [54] J. S. Tang, Z. Q. Zhou, Y. T. Wang, Y. L. Li, X. Liu, Y. L. Hua, Y. Zou, S. Wang, D. Y. He, G. Chen, Y. N. Sun, Y. Yu, M. F. Li, G. W. Zha, H. Q. Ni, Z. C. Niu, C. F. Li, and G. C. Guo, Storage of multiple single-photon pulses emitted from a quantum dot in a solid-state quantum memory, *Nat. Commun.* **6**, 9652 (2015).
- [55] Y. F. Wen, P. Zhou, Z. X. Xu, L. Yuan, H. Y. Zhang, S. Z. Wang, L. Tian, S. J. Li, and H. Wang, Multiplexed spin-wave-photon entanglement source using temporal multimode memories and feedforward-controlled readout, *Phys. Rev. A* **100**, 012342 (2019).
- [56] C. Laplane, P. Jobez, J. Etesse, N. Gisin, and M. Afzelius, Multimode and Long-Lived Quantum Correlations Between Photons and Spins in a Crystal, *Phys. Rev. Lett.* **118**, 210501 (2017).
- [57] K. Kutluer, M. Mazzera, and H. de Riedmatten, Solid-State Source of Nonclassical Photon Pairs with Embedded Multimode Quantum Memory, *Phys. Rev. Lett.* **118**, 210502 (2017).
- [58] P. Caspar, E. Verbanis, E. Oudot, N. Maring, F. Samara, M. Caloz, M. Perrenoud, P. Sekatski, A. Martin, N. Sangouard, H. Zbinden, and R. T. Thew, Heralded Distribution of Single-Photon Path Entanglement, *Phys. Rev. Lett.* **125**, 110506 (2020).
- [59] N. Jiang, Y. F. Pu, W. Chang, C. Li, S. Zhang, and L. M. Duan, Experimental realization of 105-qubit random access quantum memory, *Npj Quantum Information* **5**, 28 (2019).
- [60] Y. Pu, Y. Wu, N. Jiang, W. Chang, C. Li, S. Zhang, and L. Duan, Experimental entanglement of 25 individually accessible atomic quantum interfaces, *Sci. Adv.* **4**, 3931 (2018).
- [61] Y. F. Pu, N. Jiang, W. Chang, H. X. Yang, C. Li, and L. M. Duan, Experimental realization of a multiplexed quantum memory with 225 individually accessible memory cells, *Nat. Commun.* **8**, 15359 (2017).
- [62] M. G undođan, M. Mazzera, P. M. Ledingham, M. Cristiani, and H. de Riedmatten, Coherent storage of temporally multimode light using a spin-wave atomic frequency comb memory, *New J. Phys.* **15**, 045012 (2013).
- [63] E. Saglamyurek, M. Grimau Puigibert, Q. Zhou, L. Giner, F. Marsili, V. B. Verma, S. Woo Nam, L. Oesterling, D. Nippa, D. Oblak, and W. Tittel, A multiplexed light-matter interface for fibre-based quantum networks, *Nat. Commun.* **7**, 11202 (2016).
- [64] A. Seri, D. Lago-Rivera, A. Lenhard, G. Corrielli, R. Osellame, M. Mazzera, and H. de Riedmatten, Quantum Storage of Frequency-Multiplexed Heralded Single Photons, *Phys. Rev. Lett.* **123**, 080502 (2019).
- [65] A. Seri, A. Lenhard, D. Riel ander, M. G undođan, P. M. Ledingham, M. Mazzera, and H. de Riedmatten, Quantum Correlations between Single Telecom Photons and a Multimode On-Demand Solid-State Quantum Memory, *Phys. Rev. X* **7**, 021028 (2017).
- [66] B. Albrecht, P. Farrera, G. Heinze, M. Cristiani, and H. de Riedmatten, Controlled Rephasing of Single Collective Spin Excitations in a Cold Atomic Quantum Memory, *Phys. Rev. Lett.* **115**, 160501 (2015).
- [67] P. Vernaz-Gris, K. Huang, M. Cao, A. S. Sheremet, and J. Laurat, Highly-efficient quantum memory for polarization qubits in a spatially-multiplexed cold atomic ensemble, *Nat. Commun.* **9**, 363 (2018).

- [68] K. Surmacz, K. R. J. Nunn, K. C. Lee, V. O. Lorenz, B. Sussman, I. A. Walmsley, and D. Jaksch, Efficient spatially resolved multimode quantum memory, *Phys. Rev. A* **78**, 033806 (2008).
- [69] D. Salart, O. Landry, N. Sangouard, N. Gisin, H. Herrmann, B. Sanguinetti, C. Simon, W. Sohler, R. T. Thew, A. Thomas, and H. Zbinden, Purification of Single-Photon Entanglement, *Phys. Rev. Lett.* **104**, 180504 (2010).
- [70] L.-K. Chen, H.-L. Yong, P. Xu, X.-C. Yao, T. Xiang, Z.-D. Li, C. Liu, H. Lu, N.-L. Liu, L. Li, T. Yang, C.-Z. Peng, B. Zhao, Y.-A. Chen, and J.-W. Pan, Experimental nested purification for a linear optical quantum repeater, *Nat. Photonics* **11**, 695 (2017).
- [71] R. Reichle, D. Leibfried, E. Knill, J. Britton, R. B. Blakestad, J. D. Jost, C. Langer, R. Ozeri, S. Seidelin, and D. J. Wineland, Experimental purification of two-atom entanglement, *Nature (London)* **443**, 7113 (2006).
- [72] J.-W. Pan, S. Gasparoni, R. Ursin, G. Weihs, and A. Zeilinger, Experimental entanglement purification of arbitrary unknown states, *Nature (London)* **423**, 01623 (2003).
- [73] L. Heller, P. Farrera, G. Heinze, and H. de Riedmatten, Cold-Atom Temporally Multiplexed Quantum Memory with Cavity-Enhanced Noise Suppression, *Phys. Rev. Lett.* **124**, 210504 (2020).
- [74] I. Marcikic, H. de Riedmatten, W. Tittel, H. Zbinden, M. Legre, and N. Gisin, Distribution of Time-Bin Entangled Qubits Over 50 Km of Optical Fiber, *Phys. Rev. Lett.* **93**, 180502 (2004).
- [75] J. V. Rakonjac, D. Lago-Rivera, A. Seri, M. Mazzera, S. Grandi, and H. de Riedmatten, Entanglement between a Telecom Photon and an On-Demand Multimode Solid-State Quantum Memory, *Phys. Rev. Lett.* **127**, 210502 (2021).
- [76] Z. Xu, Y. Wu, L. Tian, L. Chen, Z. Zhang, Z. Yan, S. Li, Hai Wang, C. Xie, and K. Peng, Long Lifetime and High-Fidelity Quantum Memory of Photonic Polarization Qubit by Lifting Zeeman Degeneracy, *Phys. Rev. Lett.* **111**, 240503 (2013).
- [77] S.-Z. Wang, M.-J. Wang, Y.-F. Wen, Z.-X. Xu, T.-F. Ma, S.-J. Li, and H. Wang, Long-lived and multiplexed atom-photon entanglement interface with feed-forward controlled readouts, *Commun. Phys.* **4**, 168 (2021).
- [78] B. Albrecht, P. Farrera, X. Fernandez-Gonzalvo, M. Cristiani, and H. de Riedmatten, A waveguide frequency converter connecting rubidium-based quantum memories to the telecom C-Band, *Nat. Commun.* **5**, 3376 (2014).
- [79] R. Ikuta, T. Kobayashi, T. Kawakami, S. Miki, M. Yabuno, T. Yamashita, H. Terai, M. Koashi, T. Mukai, T. Yamamoto, and N. Imoto, Polarization insensitive frequency conversion for an atom-photon entanglement distribution via a telecom network, *Nat. Commun.* **9**, 1997 (2018).
- [80] T. van Leent, M. Bock, R. Garthoff, K. Redeker, W. Zhang, T. Bauer, W. Rosenfeld, C. Becher, and H. Weinfurter, Long-Distance Distribution of Atom-Photon Entanglement at Telecom Wavelength, *Phys. Rev. Lett.* **124**, 010510 (2020).